



## Numerical investigation on stress corrosion cracking behavior of dissimilar weld joints in pressurized water reactor plants

Lingyan Zhao

*School of Science, Xi'an University of Science and Technology, Xi'an 710054, China*

*zlblyan7878@163.com*

He Xue

*School of Mechanical Engineering, Xi'an University of Science and Technology, Xi'an 710054, China*

*Xue\_be@hotmail.com*

Fuqiang Yang

*School of Science, Xi'an University of Science and Technology, Xi'an 710054, China*

*yang\_afreet@163.com*

Yaohong Suo

*School of Science, Xi'an University of Science and Technology, Xi'an 710054, China*

*yaohongsuo@126.com*

---

**ABSTRACT.** There have been incidents recently where stress corrosion cracking (SCC) observed in the dissimilar metal weld (DMW) joints connecting the reactor pressure vessel (RPV) nozzle with the hot leg pipe. Due to the complex microstructure and mechanical heterogeneity in the weld region, dissimilar metal weld joints are more susceptible to SCC than the bulk steels in the simulated high temperature water environment of pressurized water reactor (PWR). Tensile residual stress (RS), in addition to operating loads, has a great contribution to SCC crack growth. Limited experimental conditions, varied influence factors and diverging experimental data make it difficult to accurately predict the SCC behavior of DMW joints with complex geometry, material configuration, operating loads and crack shape. Based on the film slip/dissolution oxidation model and elastic-plastic finite element method (EPFEM), an approach is developed to quantitatively predict the SCC growth rate of a RPV outlet nozzle DMW joint. Moreover, this approach is expected to be a pre-analytical tool for SCC experiment of DMW joints in PWR primary water environment.

**KEYWORDS.** Dissimilar metal weld; Stress corrosion cracking; Residual stress; Crack growth rate.

---

### INTRODUCTION

Dissimilar metal weld (DMW) joints are widely used to connect the low alloy steel (LAS) nozzles to austenitic stainless steel (SS) pipes in primary water systems of pressurized water reactors (PWR). To form a DMW joint, nickel-based alloy is generally pre-deposited on the ferritic reactor pressure vessel (RPV) nozzle face firstly, then

---

welding is carried out between the buttering layer and the pipe with nickel-based alloy. Stress corrosion cracking (SCC) of DMW joints has been paid more attention in the nuclear power industry [1]. Failures show that nickel-based alloy and its associated weld metals are more susceptible to SCC in the simulated high temperature water environments of PWR [2-4]. As a weld filler metal, the high-temperature yield strength of Alloy 182 makes it more susceptible to SCC and produce high welding residual stresses [5].

Generally, residual stresses (RS) in DMW joints are up to or even over the material yield stresses at service temperature. Tensile residual stress is one of dominant factors resulting in SCC of DMW joints [6]. RS may have a great contribution to the total stress field when pipe surface SCC in nuclear power plants is assessed. Therefore, before evaluating SCC growth at flaws in actual DMW joints of PWR plants, accurate RS distribution needs to be performed.

The film slip/dissolution oxidation model is widely regarded as a reasonable description of SCC growth estimation in the nickel-based alloys in high temperature oxygenated environment [7]. In this model, the strain rate at crack tip is usually used as a unique factor to describe the mechanical condition. Because it is difficult to directly obtain the strain rate at the steadily growing crack tip, elastic-plastic finite element method (EPFEM) is adopted to simulate the local stress-strain field and calculate the strain rate at crack tip [8]. Moreover, the SCC growth rate could be quantitatively estimated [9].

In this paper, based on the film slip/dissolution oxidation model and EPFEM, an approach is developed to quantitatively predict the SCC growth rate of a RPV outlet nozzle DMW, which services in complex operating loads and welding residual stress. Moreover, the crack driving force and the SCC behavior of the DMW joint were discussed in detail.

## CALCULATION MODEL

### *Geometry and material configuration*

The schematic of the configurations and weld geometry of a RPV outlet nozzle DMW joint is shown in Fig. 1. The hot leg pipes are typically large diameter and thick wall pipes. The outside and inside diameters of the pipe are 1001.6mm and 834.6mm, respectively, and the thickness is 83.5mm. Assume that the DMW joint consists of a low alloy steel RPV nozzle, Alloy 182 buttering, Alloy 182 weld metal and a stainless steel safe-end.

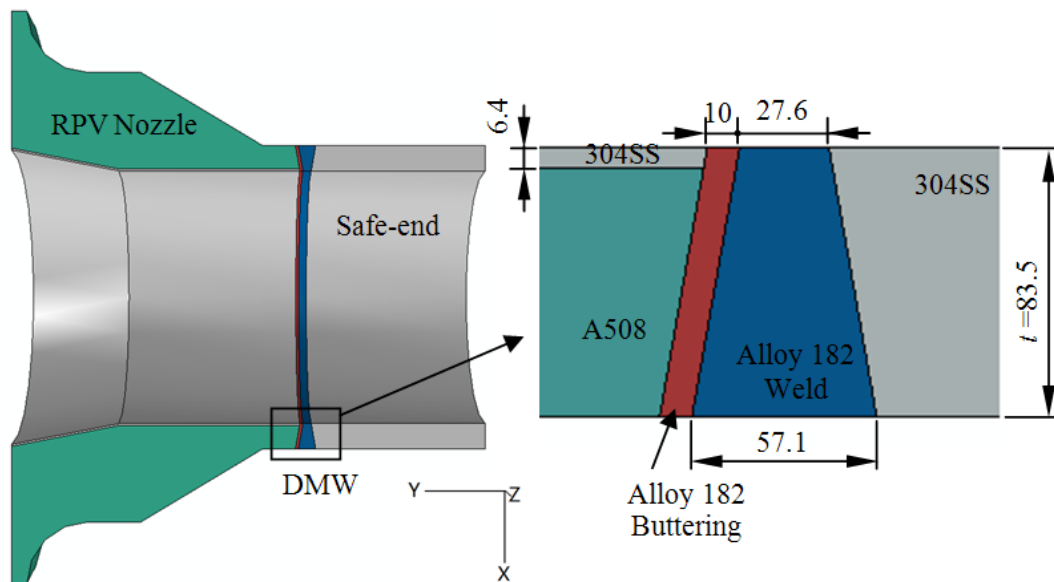


Figure 1: Geometry and material configuration of a DMW joint.

To study the cracking behavior and estimate the SCC growth rate of a representative DMW joint used in PWR, three models with small size flaws are considered in our simulation, that is, three axial semi-elliptic cracks are of different crack length ( $2c$ ) and crack depth ( $a$ ) as shown in Fig. 2 and Fig. 3. For an axial semi-elliptic crack, the crack angle ( $\theta$ ) varies from  $0^\circ$  to  $180^\circ$ . An initial axial inner surface crack having an aspect ratio ( $2c/a$ ) of 3 and a flaw depth ( $a$ ) of 5mm, 7.5mm and 10mm for the axial crack case are assumed, respectively.

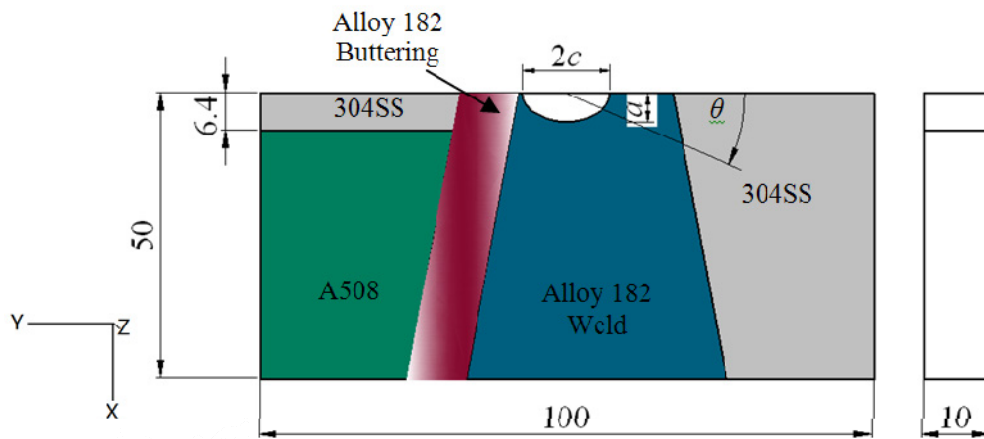


Figure 2: Geometry of the DMW joint sub-model.

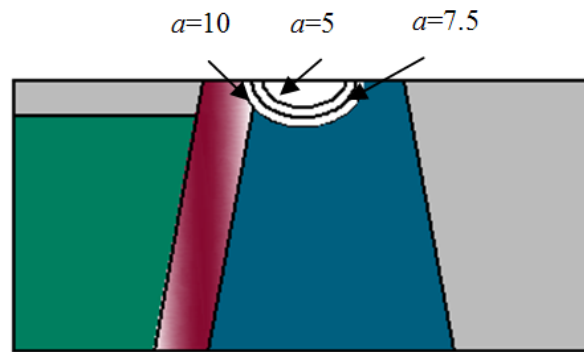


Figure 3: Crack locations and depths in the sub-model.

#### Material mechanical property of the DMW joint

The stress-strain relationship beyond yielding is represented as Romberg-Osgood equation at the loading stage, and the relationship is linearly elastic at the unloading stage in this simulation. Romberg-Osgood equation is written as:

$$\frac{\varepsilon}{\varepsilon_0} = \frac{\sigma}{\sigma_0} + \alpha \left( \frac{\sigma}{\sigma_0} \right)^n \quad (1)$$

where:

$\sigma_0$  is the yield strength of the material;

$\varepsilon_0$  is the yield strain of the material;

$\alpha$  is the dimensionless material constant;

$n$  is the strain-hardening exponent of the material.

The mechanical properties of materials are given in Tab. 1. The strain-hardening exponent of these materials is obtained in the following equation [10].

$$n = \frac{1}{\kappa \ln(1390 / \sigma_0)} \quad (2)$$

where  $\kappa=0.163$ .

The microstructure characterization of the fusion boundary region of an Alloy 182-A533B LAS dissimilar weld joint has showed that there is a narrow high hardness zone (HHZ) in the dilution zone of Alloy 182. Further, a sharp increase of the hardness was observed in the HHZ of Alloy 182 [11]. High yield stress is consistent with high hardness. Therefore, Alloy 182 buttering has higher yield stress than that of Alloy 182 weld because of the existence of HHZ.



Material	Elastic modulus, $E$ (MPa)	Poisson ratio, $\nu$	Yield stress, $\sigma_0$ (MPa)	Hardening exponent, $n$	Constant, $\alpha$
A508	193000	0.288	440	5.333	1.0
Alloy 182 Buttering	193000	0.288	480	5.769	1.0
Alloy 182 Weld	193000	0.288	385	4.779	1.0
304SS	193000	0.288	254	4.402	1.0

Table 1: Material mechanical parameters for the FEM simulation.

*Residual stress and operating loads*

Only the hoop stress is used in the current evaluation based on some assumptions because the pipe flaw is an axial crack. The distribution of residual stress [12] is shown in Fig.4. Note that only the hoop stress for an axial crack was applied in the weld region.

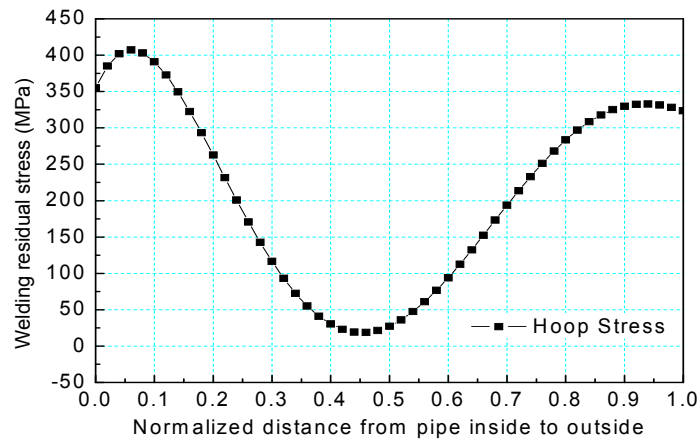


Figure 4: Welding residual stress profiles.

Normal operating loads for RPV nozzles are listed in Tab. 2. In addition to that, both axial and hoop stresses varying through-thickness induced by internal fluid pressure are considered. The welding residual stress applied as field and remote bending moment are also taken into account.

Service temperature [13] (°C)	Inner pressure (MPa)	Axial pressure (MPa)	Bending moment (kNm)	Welding residual stress (MPa)
345	15.59	44	2 492	Shown in Fig. 4

Table 2: Normal operating loads for RPV nozzles.

*FEM model*

A commercial FEM code, ABAQUS, was used in this simulation analysis. Based on symmetry condition, half of the model was investigated. The pipe symmetry surface is symmetric restrained in X-Y plane. Appropriate extensions of the left and right ends in the model have been made to reduce the influence of edge effect on the analysis results. Considering the nozzle and pressure vessel are rigidly connected, the fixed constraint on the left is set. The combined operating loads such as internal pressure, weight and moment loads are applied on the safe end DMW joint.

Sub-model technique was adopted to investigate the crack local stress-strain field in detail. With different sampling location, three models are calculated based on the sub-model technique. Boundaries of the sub-model are driven by the stress-strain obtained from the global model analysis [14].

Fig.5 gives the mesh of a DMW joint specimen (global model and sub-mode), where X-Y datum is the crack surface and Z-axis is the crack growth direction. Mesh at the vicinity of crack front is observably refined in both global model and

sub-model. 90387 and 46110 8-node linear brick elements are adopted in the global model and sub-model, respectively. There are 28020 elements in the vicinity of 2 mm around the crack front in the sub-model, more than the half the element total number. The minimum size of the element is about 0.02mm in the sub-model.

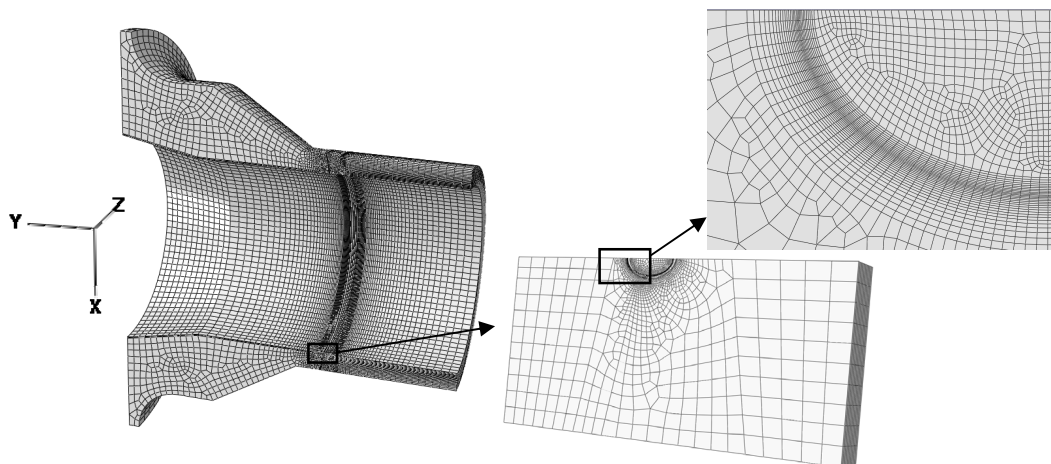


Figure 5: Mesh of the finite element model.

## RESULTS AND DISCUSSIONS

Mechanical factors, such as crack opening stress, plastic strain and  $J$ -integral ahead of crack front, are always important to discuss the SCC crack growth behaviors. To quantitatively estimate SCC growth rate of the flaws in DMW joints, the local opening stress, plastic strain and  $J$ -integral ahead of crack front are investigated in this section.

### *Distributions of the hoop stress and hoop strain*

The hoop stress and the hoop plastic strain are shown in Fig. 6 and Fig. 7, respectively. It is obvious that the effect of operating loads on the DMW joint containing defects is much smaller than that of residual stress. Only operating loads (OL) applied, the hoop stress and strain is linear along pipe through-thickness. Comparing Fig. 4 with Fig. 6, the hoop stress induced by RS and OL is not a simple summation of that induced by hoop RS and OL due to the high stress, which exceeds the yield stress of Alloy 182 weld. Under the combined effects of RS and operating loads, the distribution of hoop stress and hoop strain along pipe through-thickness is consistent with that of hoop residual stress in Fig. 4.

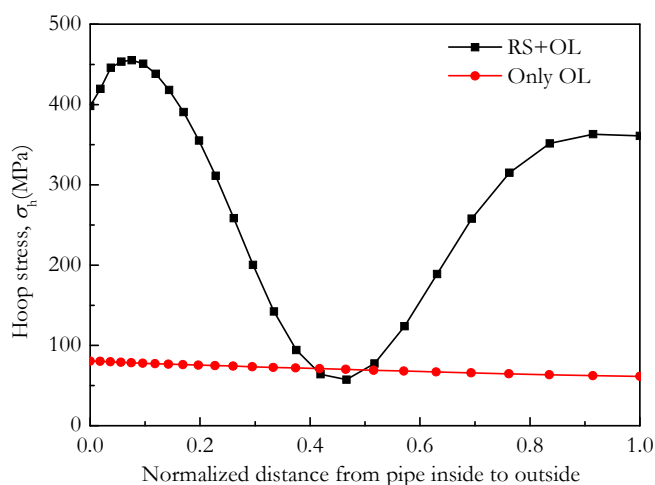


Figure 6: Hoop stress along pipe through-thickness.

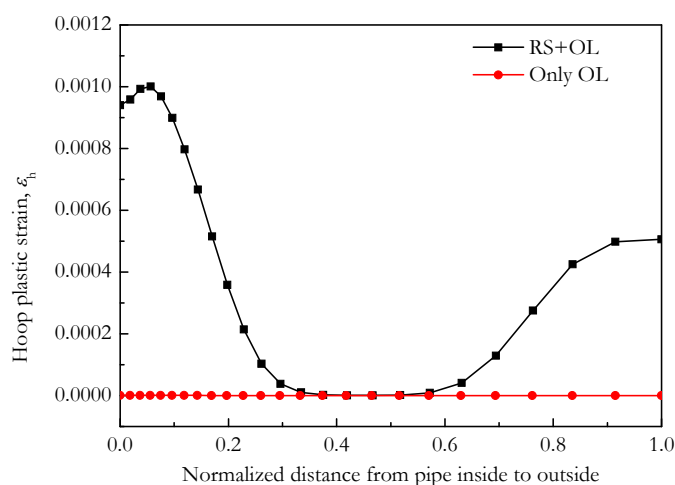


Figure 7: Hoop strain along pipe through-thickness.

*Distributions of stress and strain ahead of crack fronts*

Crack tip strain  $\epsilon_{ct}$  is the main mechanical parameter affecting SCC growth rate in Ford's model [15], which is widely used in analyzing SCC behavior of key materials in PWR components. Because it is difficult to directly obtain  $\epsilon_{ct}$ , plastic strain  $\epsilon_p$  was used to replace  $\epsilon_{ct}$  at a characteristic distance  $r_0$  ahead of crack tip in FRI model [16]. Thus, the critical issue is to estimate  $r_0$  when SCC growth rate is predicted. Considering that the mechanical field near crack front is pertinent to SCC growth,  $r_0$  is regarded to be smaller than the plastic zone size.

Strain and strain rate quickly decrease with the increasing  $r_0$ . On the other hand, the error in numerical calculation is very big at the crack tip because of the stress-strain singularity near the crack tip. Considering the above factors and comparing the crack tip plastic zones where the equivalent plastic strain is 0.2% with different crack depths, the reasonable distance from crack front is designated as  $60\mu\text{m}$  in this paper.

In Fig. 8 and Fig. 9, the opening stress and normal plastic strain at a characteristic distance ( $r_0=60\mu\text{m}$ ) ahead of crack front are observably small when the crack depth is 5mm. The difference between yield stresses of interface materials lead to the jump of opening stress along crack fronts in Fig. 8 could be explained that for 7.5 and 10 mm cracks the crack passes Alloy 182 buttering, where contains much higher yield stress. The opening stress and normal plastic strain for 7.5 and 10mm crack make little difference. These results suggest that the normal plastic strain ahead of deeper crack front has a smaller gradient.

The stress and strain are symmetrically distributed ahead of crack front when the crack depth is 5mm. For the partial crack in Alloy 182 buttering, the opening stress ahead of the crack front ( $a=7.5\text{mm}$  and  $\theta=150^\circ$ ) increases sharply, whereas the strain decreases. As the crack grows, the opening stress ahead of the crack front ( $a=10\text{mm}$  and  $\theta=120^\circ$ ) becomes larger. The effect of crack depth on the stress ahead of crack fronts is more dramatic than it on the strain.

At the interfacial region between Alloy 182 buttering and Alloy 182 weld, the stresses ahead of crack fronts suddenly increase while the strains decrease due to different material yield stresses of the two sides. Under the same loading condition, the equivalent stress intensity factor ahead of crack front increases with crack length. The increment of stress ahead of crack front, which increases with the applied loads, is connected with the yield stresses of interface materials.

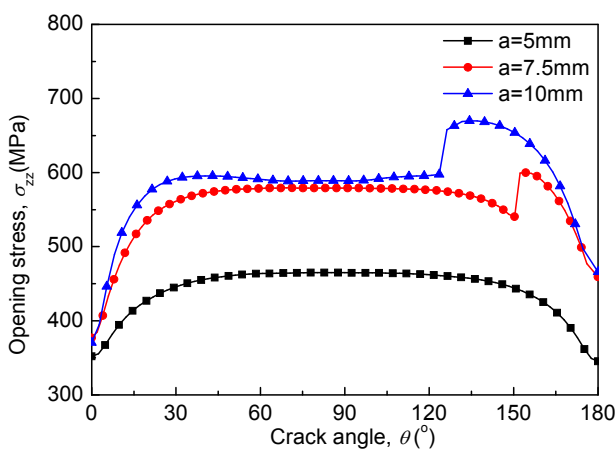


Figure 8: Opening stress ahead of crack fronts ( $r_0=60\mu\text{m}$ ).

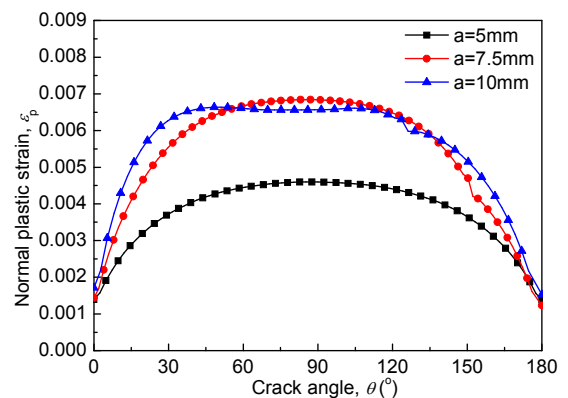


Figure 9: Normal plastic strain ahead of crack fronts ( $r_0=60\mu\text{m}$ ).

Cracks are mainly located in the high residual stress region when the crack depth varies from 5mm to 10mm. Thus, residual stress has a great influence on stress and strain ahead of crack front. The local stress-strain field of shallow surface crack is dominated by RS, not the welded mechanical heterogeneity. The effect of residual stress on crack local stress and strain will become smaller with deeper crack.

*Normal plastic strain rates and J-integrals*

Normal plastic strain rates and  $J$ -integrals ahead of the crack fronts can be seen in Fig. 10 and Fig. 11, respectively. Located in the middle of a homogeneous material Alloy 182 weld, the stress, plastic strain, plastic strain rate and  $J$ -integral ahead of crack front are minimal and of the same trend when the crack length is 5mm. The normal plastic strain rate is higher at the deepest point than each end of the crack front. Correspondingly, the growth rate at the deepest point of the

crack front is the highest. The strain rate increments significantly decrease with the increasing crack depth, which indicates that the deep surface crack growing slow down.

The  $J$ -integral is not increasing with crack length (from 7.5 mm to 10 mm) in Fig. 11 because the hoop stress that causes the crack opening is decreasing (normalized distance from 0.09 to 0.125) in Fig. 4 with crack length (from 7.5 mm to 10 mm). That is, the loading conditions (mainly the RS) are different when the crack length is 7.5 mm and 10 mm. The increase of  $J$ -integral should be offset by the decrease of crack driving force.

The distributions of strain rate and  $J$ -integral ahead of deeper surface crack front are quite different in the interfacial region of Alloy 182 buttering and Alloy 182 weld. The strain rate decreases due to the constraint of material with high hardness while  $J$ -integral increases in the interfacial region. Some researchers discovered that the mechanical properties of welded joints had many distinct characteristics compared with homogeneous materials, especially for the fracture properties. Path dependence of  $J$ -integral exists because of the finite deformation in the vicinity of crack tip and the heterogeneous mechanical properties of welded joint. Therefore, there are some doubts on the applications of  $J$ -integral in heterogeneous DMW joints [17]. The plastic strain rate should be a more reliable fracture parameter to evaluate the SCC behavior of DMW joint than  $J$ -integral.

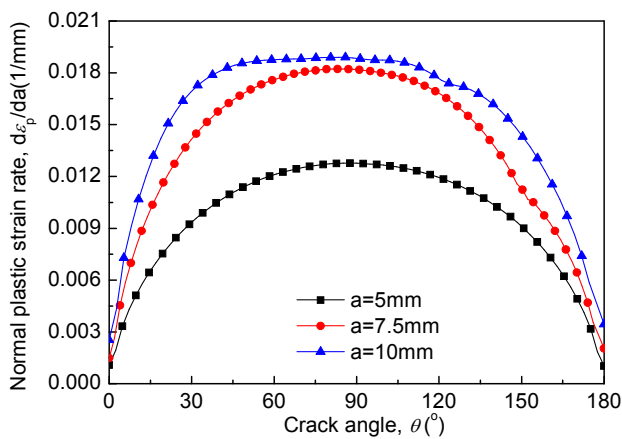


Figure 10: Normal plastic strain rate ahead of crack fronts ( $r_0=60\mu\text{m}$ ).

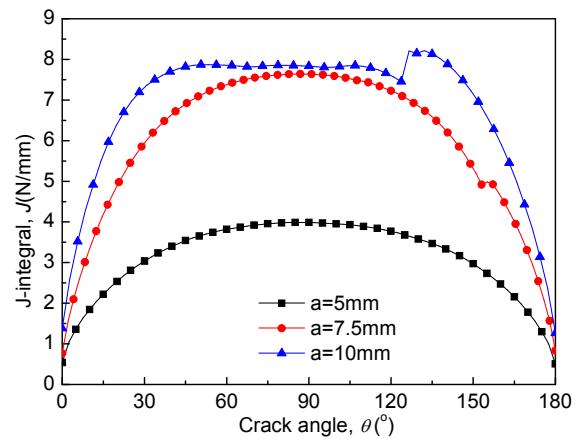


Figure 11:  $J$ -integral ahead of crack fronts.

### SCC growth rate

In order to predict the amount of time required before leakage occurs in normal PWR, a detailed prediction on stress corrosion cracking growth rate of DMW joints are performed by many researchers. Generally, stress corrosion cracking growth law for Alloy 82/182 weld metals in PWR primary water environment has been described as a function of applied stress intensity factor  $K_I$  and thermal activation corrosion term: temperature, based upon the extensive SCC material testing data [18]. These correlations provide the flaw evaluation guidelines for Ni-based alloy materials in PWR environment.

The stress intensity factor  $K_I$  along the crack front in the elastic-plastic material is converted by the value of  $J$ -integral. However, there are some doubts on the applications of  $J$ -integral along interface crack front in heterogeneous DMW joints. Combined with EPFEM, a pre-analytical method is used to predict SCC growth rate of DMW joints in PWR environment.

The stress corrosion cracking growth rate can be written as:

$$\frac{da}{dt} = \kappa'_a \cdot \left(\frac{d\varepsilon_p}{da}\right)^{\frac{m}{1-m}} \quad (3)$$

where the oxidation rate constant  $\kappa'_a$  is  $7.478 \times 10^{-7}$ , the exponent of current decay curve  $m$  is 0.5 [19].

Fig. 10 shows the normal plastic strain rate at a characteristic distance ( $r_0=60\mu\text{m}$ ) ahead of the crack fronts. Based on the normal plastic strain rates and the formula, SCC growth rate evaluations were performed for Alloy182 weld metal conservatively at a service temperature of 345°C. The disposition curves of SCC growth rate are shown in Fig. 12. The units describe crack growth rate in terms of millimeter per second. Note that for the axial crack case, because low alloy



steel and stainless steel have significantly lower SCC susceptibilities and growth rates, the crack growth law was only applied to the partial model including Alloy182 buttering and Alloy182 weld.

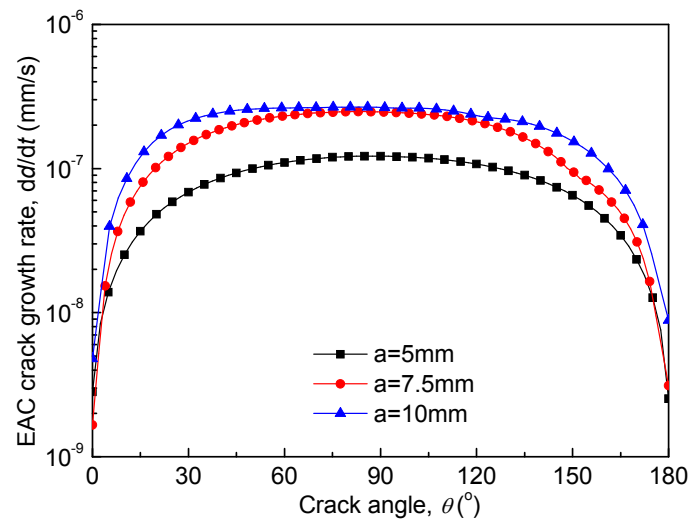


Figure 12: Crack growth rate of Alloy 182 in the DMW joint.

The shallow surface crack growth rate at both ends is much lower than that at the middle. However, the deep surface crack growth rate is relatively uniform and its increment slows down with the increasing crack depth. The gradients of plastic strain and plastic strain rates decrease as the crack advances. Due to the constraint of strong material, CGR of the deep surface crack locates in Alloy 182 buttering decreases sharply, and the crack growing in Alloy 182 buttering is inhibited. However, the partial crack locates in Alloy 182 weld comes to stable growth. The crack will no longer be ideal semi-elliptic with the continuous crack growing. The crack shape will change considerably.

The welding residual stress referred here is a result of higher hoop stress in the DMW joint SCC susceptible region, and dropping off in the safe-end and nozzle regions. Finally, the crack shape development results in crack growth outside of the DMW region.

## CONCLUSIONS

Considering the interactive effect of operating loads and welding residual stress, the stress-strain field ahead of inner surface axial crack fronts of a RPV outlet nozzle DMW joint is simulated by using EPFEM. The crack driving force, such as opening stress, plastic strain, plastic strain rate and  $J$ -integral are analyzed. Focusing on RS and crack depth, the SCC growth rate of a DMW joint was quantitatively predicted. Main conclusions can be summarized as follows:

- (1) Crack local stress-strain field,  $J$ -integral and crack growth rate of DMW joints are dominated by residual stress, not welded mechanical heterogeneity. The hoop stress and hoop strain varying through-thickness of the welded area is quite different with or without residual stress. The distributions of hoop stress and hoop strain are consistent with residual stress.
- (2) The strain rate ahead of deeper crack front decreases due to the constraint of high hardness material, whereas,  $J$ -integral increases in the interfacial region of Alloy 182 buttering and Alloy 182 weld. Path dependence of  $J$ -integral exists because of welded mechanical heterogeneity. Therefore, plastic strain rate should be a more reliable fracture parameter to evaluate the SCC behavior of DMW joint than  $J$ -integral.
- (3) The shallow surface crack growth rate at both ends is much lower than that at the middle. However, the deep surface crack growth rate is relatively uniform. Due to the constraint of strong material, located in Alloy 182 buttering, the crack growing is inhibited. The crack locates in Alloy 182 weld grows steady and the crack shape will change considerably.
- (4) Based on the film slip/dissolution oxidation model and EPFEM, a valid approach is provided to quantitatively estimate SCC growth rate of DMW joints in PWR environment.



## ACKNOWLEDGEMENTS

The supports from Natural Science Foundation of China (Grants Nos. 11072191 and 1201277), Scientific Research Program Funded by Shaanxi Provincial Education Commission (Program Nos. 12JK0851 and 2013JK0611) and Research Fund for the Doctoral Program of Higher Education of China (Grants Nos. 20136121110001) are appreciated.

## REFERENCES

- [1] Bamford, W., Hall, J., A review of Alloy 600 cracking in operating nuclear plants including Alloy 82 and 182 weld behavior, ASME 12<sup>th</sup> International Conference on Nuclear Engineering, (2004) 131–139.
- [2] Bamford, W., Newton, B., Seeger, D., Recent experience with weld overlay repair of indications in alloy 182 butt welds in two operating PWRs, ASME 2006 Pressure Vessels and Piping Conference, (2006) 427–434.
- [3] Li, G.F., Congleton, J., Stress corrosion cracking of a low alloy steel to stainless steel transition weld in PWR primary waters at 292°C, *Corros. Sci.*, 42(6) (2000) 1005–1021.
- [4] Li, G.F., Li, G.J., Fang, K.W., Stress corrosion cracking behavior of dissimilar metal weld A508/52M/316L in high temperature water environment, *Acta Metallurgica Sinica*, 47(7) (2011) 797–803.
- [5] Andresen, P.L., Young, L.M., Emigh, P.W., et al., Stress corrosion crack growth rate behavior of Ni Alloys 182 and 600 in high temperature water, *NACE Corrosion*, (2002) 02510.
- [6] Deng, D., Kiyoshima, S., FEM prediction of welding residual stresses in a SUS304 girth-welded pipe with emphasis on stress distribution near weld start/end location, *Comp. Mater. Sci.*, 50(2) (2010) 612–621.
- [7] Andresen, P.L., Environmentally assisted growth rate response of nonsensitized AISI 316 grade stainless steels in high temperature water, *Corrosion*, 44(7) (1988) 450–460.
- [8] Xue, H., Ogawa, K., Shoji, T., Effect of welded mechanical heterogeneity on local stress and strain in stationary and growing crack tips, *Nucl. Eng. Des.*, 236(5) (2009) 628–640.
- [9] Xue, H., Shoji, T., Quantitative prediction of EAC crack growth rate of sensitized type 304 stainless steel in boiling water reactor environments based on EPFEM, *J. Press. Vess.-T. ASME*, 129(3) (2007) 460–467.
- [10] Ueda, Y., Shi, Y., Sun, S., et al., Effect of crack depth and strength mis-matching on the relation between J-integral and CTOD for welded tensile specimens (mechanics, strength & structure design), *Trans. JWRI*, 26(1) (1997) 133–140.
- [11] Peng, Q.J., Xue, H., Hou, J., et al., Role of water chemistry and microstructure in stress corrosion cracking in the fusion boundary region of an Alloy 182-A533B low alloy steel dissimilar weld joint in high temperature water, *Corros. Sci.*, 53(12) (2011) 4309–4317.
- [12] Hayashi, T., Hankinson, S.F., Saito, T., et al., Flaw evaluation for PWR and BWR component weld joints using advanced FEA modeling techniques, ASME 2009 Pressure Vessels and Piping Conference, (2009) 1125–1139.
- [13] Lu, Z.P., Shoji, T., Xue, H., et al., Deterministic formulation of the effect of stress intensity factor on PWSCC of Ni-base alloys and weld metals, *J. Press. Vess.-T. ASME*, 135(2) (2013) 021402.
- [14] ABAQUS v6.7, Hibbitt, Karlsson and Sorensen Inc, (2007).
- [15] Ford, P., Mechanisms of environmentally-assisted cracking, *Int. J. Pres. Ves. Pip.*, 40(55) (1989) 343–362.
- [16] Shoji, T., Li, G., Kwon, J., et al., Quantification of yield strength effects on IGSCC of austenitic stainless steels in high temperature water, *Proceedings of the 11th Conference of Environmental Degradation of Materials in Materials in Nuclear Systems*, (2003) 834–844.
- [17] Kang, J.D., Wen, W.D., Zhang, Y.F., et al., Path dependence of J-integral in welded joint with an overmatching weld, *Trans. of NUAA*, 12(1) (1995) 1–8.
- [18] Xue, H., Sato, Y., Shoji, T., Quantitative estimation of the growth of environmentally assisted cracks at flaws in light water reactor components, *J. Press. Vess.-T. ASME*, 131(1) (2009) 011404.
- [19] Peng, Q.J., Kwon, J., Shoji, T., Development of a fundamental crack tip strain rate equation and its application to quantitative prediction of stress corrosion cracking of stainless steels in high temperature oxygenated water, *J. Nucl. Mater.*, 324(1) (2004) 52–61.